An energetic perspective on hydrological cycle changes in the Geoengineering Model Intercomparison Project

Ben Kravitz,[1] Philip J. Rasch,[1] Piers M. Forster,[2] Timothy Andrews,[3] Jason N. S. Cole,[4] Peter J. Irvine,[5] Duoying Ji,[6] Jón Egill Kristjánsson,[7] John C. Moore,[6] Helene Muri,[7] Ulrike Niemeier,[8] Alan Robock,[9] Balwinder Singh,[1] Simone Tilmes,[10] Shingo Watanabe,[11] and Jin-Ho Yoon[1]

Received 9 July 2013; revised 15 November 2013; accepted 22 November 2013; published 11 December 2013.

[1] Analysis of surface and atmospheric energy budget responses to CO_2 and solar forcings can be used to reveal mechanisms of change in the hydrological cycle. We apply this energetic perspective to output from 11 fully coupled atmosphere-ocean general circulation models simulating experiment *G1* of the Geoengineering Model Intercomparison Project (GeoMIP), which achieves top-of-atmosphere energy balance between an abrupt quadrupling of CO_2 from preindustrial levels (*abrupt4xCO2*) and uniform solar irradiance reduction. We divide the climate system response into a *rapid adjustment*, in which climate response is due to adjustment of the atmosphere and land surface on short time scales, and a *feedback response*, in which the climate response is predominantly due to feedback related to global mean temperature changes. Global mean temperature change is small in *G1*, so the feedback response is also small. *G1* shows a smaller magnitude of land sensible heat flux rapid adjustment than in *abrupt4xCO2* and a larger magnitude of latent heat flux adjustment, indicating a greater reduction of evaporation and less land temperature increase than *abrupt4xCO2*. The sum of surface flux changes in *G1* is small, indicating little ocean heat uptake. Using an energetic perspective to assess precipitation changes, *abrupt4xCO2* shows decreased mean evaporative moisture flux and increased moisture convergence, particularly over land. However, most changes in precipitation in *G1* are in mean evaporative flux, suggesting that changes in mean circulation are small.

Citation: Kravitz, B., et al. (2013), An energetic perspective on hydrological cycle changes in the Geoengineering Model Intercomparison Project, *J. Geophys. Res. Atmos.*, *118*, 13,087–13,102, doi:10.1002/2013JD020502.

1. Introduction

[2] Solar geoengineering, also known as Solar Radiation Management, has been proposed as a means of reducing some of the climate effects of increased concentrations of carbon dioxide by reducing the amount of incident insolation [e.g., *Crutzen*, 2006; *Shepherd et al.*, 2009]. However, the compensation of greenhouse gas forcing by solar geoengineering, especially on a local scale, is imperfect [e.g., *Robock et al.*, 2008; *Ricke et al.*, 2010; *Moreno-Cruz et al.*, 2012]. Should society develop the will to deploy geoengineering, understanding of the expected climate effects will likely play a key role in the discussion of how deployment might be performed and governed.

[3] One of the key areas of concern regarding the climate effects of geoengineering is the potential effects on the hydrological cycle. *Trenberth and Dai* [2007] and *Robock et al.* [2008] provided strong observational and model-based evidence that a reduction of the intensity of the hydrological cycle is a plausible side effect from geoengineering with stratospheric sulfate aerosols. Furthermore, *Haywood et al.* [2013] showed that stratospheric sulfate aerosol geoengineering in only one hemisphere can shift the location

Additional supporting information may be found in the online version of this article.

[1]Atmospheric Sciences and Global Change Division, Pacific Northwest National Laboratory, Richland, Washington, USA.
[2]School of Earth and Environment, University of Leeds, Leeds, United Kingdom.
[3]Met Office Hadley Centre, Exeter, United Kingdom.
[4]Canadian Centre for Climate Modelling and Analysis, Environment Canada, Toronto, Ontario, Canada.
[5]Institute for Advanced Sustainability Studies, Potsdam, Germany.
[6]State Key Laboratory of Earth Surface Processes and Resource Ecology, College of Global Change and Earth System Science, Beijing Normal University, Beijing, China.
[7]Department of Geosciences, University of Oslo, Oslo, Norway.
[8]Max Planck Institute for Meteorology, Hamburg, Germany.
[9]Department of Environmental Sciences, Rutgers University, New Brunswick, New Jersey, USA.
[10]National Center for Atmospheric Research, Boulder, Colorado, USA.
[11]Japan Agency for Marine-Earth Science and Technology, Yokohama, Japan.

Corresponding author: B. Kravitz, Atmospheric Sciences and Global Change Division, Pacific Northwest National Laboratory, 902 Battelle Boulevard, PO Box 999, MSIN K9-24, Richland, WA 99352, USA. (ben.kravitz@pnnl.gov)

2169-897X/13/10.1002/2013JD020502

of the Intertropical Convergence Zone, altering tropical precipitation patterns, including Sahelian precipitation. To determine robust climate model responses to geoengineering, the Geoengineering Model Intercomparison Project (GeoMIP) was initiated [*Kravitz et al*., 2011]. Under this framework, several intercomparisons of simulated effects on precipitation have been performed [*Schmidt et al*., 2012; *Jones et al*., 2013; *Kravitz et al*., 2013; *Tilmes et al*., 2013]. Insolation reduction reduces both global precipitation (P) and evaporation (E); model results indicate few net changes in $P-E$ in many regions [*Schmidt et al*., 2012; *Kravitz et al*., 2013]. Changes in monthly precipitation extremes experienced under climate change [e.g., *Held and Soden*, 2006] are suppressed in simulations using insolation reduction to compensate for CO_2 radiative forcing, especially over monsoonal reasons [*Tilmes et al*., 2013].

[4] Traditional temperature and moisture perspectives are useful for determining hydrological cycle changes in specific simulations. The underlying mechanisms describing the changes can be revealed through an analysis of the surface and atmospheric energy budgets. The energetic perspective has been shown to reveal key features of climate model response to both CO_2 increases and solar irradiance changes [e.g., *Andrews et al*., 2009; *Bala et al*., 2010; *Cao et al*., 2012]. This perspective has also been preliminarily applied to geoengineering, particularly balancing the radiative forcing from a CO_2 increase with a reduction in solar irradiance. Using an atmospheric model coupled to a slab ocean model, *Bala et al*. [2008] showed how the changes in globally averaged equilibrium surface radiative fluxes due to geoengineering are primarily balanced by changes in latent heat flux, resulting in a decrease in global mean evaporation.

[5] Here we extend and expand upon the analyses of *Schmidt et al*. [2012] to 11 models participating in GeoMIP (see *Kravitz et al*. [2013, Table 1] for model details and Table S1 of this paper to determine which models are incorporated in the analysis presented here). We follow the analysis methods of *Bala et al*. [2008], but use of fully coupled atmosphere-ocean general circulation models instead of slab ocean models allows us to assess the response of the surface and atmospheric energy budgets over different time scales (see section 3 below). We also assess contrasts between radiative responses over land and ocean, yielding important clues about the land/sea contrast of hydrological cycle changes and an assessment of the potential for ocean heat uptake. Furthermore, we use these calculations of surface and atmospheric energy fluxes to apply for the first time the energetic perspective of *Muller and O'Gorman* [2011] (see section 5) to geoengineering simulations. This formulation aids in attributing precipitation changes on both a global and local scale to changes in mean evaporative moisture flux and changes in the mean circulation. By using a large multimodel ensemble to assess these changes, we can determine the robustness of our findings.

[6] In section 2, we discuss the experimental design and our methods of analysis. In section 3, we discuss differentiation of time scales, particularly a separation into a rapid adjustment term and a feedback response term. In section 4, we characterize changes in the surface and atmospheric energy budgets, assessing both instantaneous and time-varying responses. In section 5, we use this understanding of changes in the surface and atmospheric energy budgets to interpret changes in precipitation flux. Section 6 contains a discussion of our results, conclusions from our study, and provides a greater context for our findings.

2. Experiment Design and Analysis

[7] The analyses presented here are based on the same experiments discussed by *Kravitz et al*. [2013] and *Tilmes et al*. [2013]. The control simulation, denoted *piControl*, is a simulation of steady state preindustrial conditions. *abrupt4xCO2* is the standard Coupled Model Intercomparison Project Phase 5 (CMIP5) simulation in which CO_2 concentrations are instantaneously quadrupled from preindustrial levels to ~1140 ppm [*Taylor et al*., 2012]. *G1* is the GeoMIP experiment in which a solar irradiance reduction is imposed upon a background *abrupt4xCO2* scenario such that top-of-atmosphere (TOA) radiative flux is negligible (< 0.1 W m^{-2}) [*Kravitz et al*., 2011].

[8] In this paper, all radiative and turbulent fluxes are reported as positive in the downward direction. All changes are relative to an average of all years of *piControl* for each model. When reported in the body of the text, values are given as "mean (min to max)" where "mean" denotes the all-model ensemble mean (calculated for each experiment as an average of all models weighted equally), "min" denotes the minimum value of that quantity among all models, and "max" denotes the maximum value of that quantity among all models. Model agreement is defined to be a region or grid box where at least 75% of the models (Table S1) agree on the sign of the change (difference from *piControl*) of that quantity. For quantities given as ratios, e.g., the Bowen ratio (described below), model agreement is defined to be a region where at least 75% of the models agree whether the ratio either increases or decreases. If models agree over a region, the climate response in that region is stated to be robust. Areas in map plots that are not robust are stippled to obscure those regions. Values corresponding to the all-model ensemble mean and model range are listed in Tables S3–S8, although the tables are not explicitly mentioned when characterizing model results; these tables complement the comparatively qualitative descriptions in sections below.

[9] Tables S7 and S8 show changes in radiative fluxes over different regions of the globe. The Arctic is defined as all grid boxes North of 66.55°N. The Antarctic is all grid boxes South of 66.55°S. The polar region is defined to be an average of the Arctic and Antarctic. The tropics are all grid boxes between 23.44°S and 23.44°N. The midlatitudes are all regions between the tropics and the poles.

[10] This work concentrates only on annually averaged quantities. Many of the radiative quantities discussed in subsequent sections will undoubtedly have a seasonal cycle that could be modulated by geoengineering, particularly if the CO_2 physiological effect (described in subsequent sections) is included. However, these changes are expected to be sufficiently complex as to distract from the main findings, so discussions of the seasonal cycle are reserved for future work.

[11] All results described in subsequent sections are specific to the highly idealized experiment design. However, as described in detail by *Kravitz et al*. [2013], this experiment can yield important clues and reveal fundamental understanding of climate processes and responses to other geoengineering scenarios. The way in which geoengineering would be performed strongly depends on the desired climate goal, so

the purpose here is not to provide a perfectly realistic representation of geoengineering, but instead to improve understanding and promote ease of model intercomparison; the experiments discussed here are well suited to this purpose.

3. Differentiation of Response Time Scales

[12] Climate system response is divided into two broad time scales, termed the *rapid adjustment* and *feedback response*, also called the fast and slow responses, respectively. The response of the climate system to a forcing operates on multiple time scales due to different response times in parts of the climate system [*Andrews and Forster*, 2010]. Because the atmosphere and parts of the land surface have a low heat capacity, they adjust quickly in response to forcing; these responses, termed rapid adjustments, are unassociated with changes in global mean surface air temperature [*Andrews et al*., 2009; *Bala et al*., 2010; *Cao et al*., 2012]. On longer time scales, the land and ocean surface will warm, and any global climate system response to these warming temperatures is termed the feedback response.

[13] Rapid adjustments generally occur within the first few weeks or months of the *abrupt4xCO2* and *G1* simulations [*Cao et al*., 2012; *Dong et al*., 2009]. To isolate these adjustments from the climate response to temperature increases, the rapid adjustment is defined here as quantities averaged over the first year of simulation. We acknowledge deficiencies in this definition, in that results may be contaminated by some global temperature change (see below). Part of the feedback response is captured in an average over years 11–50, as in *Kravitz et al*. [2013] and *Tilmes et al*. [2013]. Because changes in the ocean mixed layer operate on a time scale of approximately 10 years [e.g., *Gregory and Forster*, 2008; *Jarvis*, 2011], averaging over the chosen period is sufficient to capture some of the response of the climate system to changes in temperature. However, over this period, the rapid adjustment and feedback responses of the climate system are convolved [e.g., *Bala et al*., 2010]. To isolate the feedback response from the rapid adjustment, the year 1 average is subtracted from the years 11–50 average; this difference is defined here as the feedback response. Because different models may vary in their radiative adjustment times, averaging over subyear time scales would likely exacerbate intermodel differences and amplify seasonal cycle variability, obscuring results, and preventing consistent analysis. Using the first full year as a representation of model rapid adjustment is a compromise that allows us to assess the radiative effects for small amounts of temperature change, but independent of the seasonal cycle, thus capturing the essence of the quantities we wish to analyze.

[14] This method of representing the feedback response is similar to the approach of *Schmidt et al*. [2012], although they reported feedback response changes for *abrupt4xCO2* as averages over years 101–150, whereas we report changes over years 11–50. Although our method truncates some of the warming that will be realized, as well as some of the feedbacks operating on longer time scales, analysis over this shorter period is sufficient to differentiate the rapid adjustment and feedback responses, allowing accurate description of qualitative differences between radiative responses and temperature-related feedbacks. The method used here also has the advantage of representing consistent quantities in both *abrupt4xCO2* and *G1*, as *G1* was only simulated for 50 years by most modeling groups.

[15] These divisions into rapid adjustment and feedback responses are imperfect, as some amount of temperature change, particularly in the *abrupt4xCO2* simulation, will be realized in the first year of simulation [*Dong et al*., 2009; *Kravitz et al*., 2013; *Tilmes et al*., 2013]. Often, the rapid adjustment is determined by the ordinate intercept obtained from regression of annually averaged changes in radiative fluxes against changes in temperature, and the feedback response is given by the slope of the regression line, expressed as radiative flux changes relative to temperature changes [*Gregory et al*., 2004]. This method is well suited to determining rapid adjustment and feedback responses in *abrupt4xCO2*, but is inapplicable to *G1*, because changes in globally averaged surface air temperature are very small [*Kravitz et al*., 2013]. The method chosen here can be applied to both *abrupt4xCO2* and *G1* but may be somewhat inaccurate in determining the rapid adjustments in both simulations.

[16] To determine the effects of this choice of representing the rapid adjustments, we analyzed radiative fluxes for the *sstClim* and *sstClim4xCO2* simulations from six of the models participating in GeoMIP (see Table S1 for participating models). *sstClim* is a preindustrial control simulation with prescribed sea surface temperatures and sea ice. *sstClim4xCO2* involves prescribed preindustrial sea surface temperatures and sea ice in which CO_2 concentrations are instantaneously quadrupled; this simulation can be seen as an intermediate simulation between *sstClim* and *abrupt4xCO2*. Because these simulations have fixed sea surface temperatures, they contain no feedback response, meaning an average over all years of radiative flux changes (*sstClim4xCO2–sstClim*) will give a good estimate of the rapid adjustment in these models. The results of the six-model ensemble mean are given in Table S2.

[17] Overall, our method of estimating the rapid adjustment shows good agreement with values obtained from simulations with fixed sea surface temperatures. The longwave response (averaged over year 1) is slightly higher than in the fixed sea surface temperature simulations, which is to be expected if the results include a small amount of temperature change. The largest differences are found in latent heat flux changes; the annual average of the first year captures less than half of the latent heat response obtained from the simulations with fixed sea surface temperatures. This in turn affects estimates of the surface energy budget (see section 4.3 and equation (1) below) and radiative estimates of evaporation changes (see section 5.1 and equation (5) below). Although our method of representing the rapid adjustment fails to capture the full magnitude of the latent heat rapid adjustment in *abrupt4xCO2*, it does capture the qualitative behavior of latent heat flux changes. Thus, this compromise does not affect our conclusions, although care must be taken in interpreting the results presented here, particularly when comparing relative magnitudes of different radiative fluxes.

4. Changes in the Surface Radiation Budget

[18] The radiation budget at the top of the atmosphere is comprised of shortwave and longwave components. At the surface, any changes in radiative fluxes are compensated by

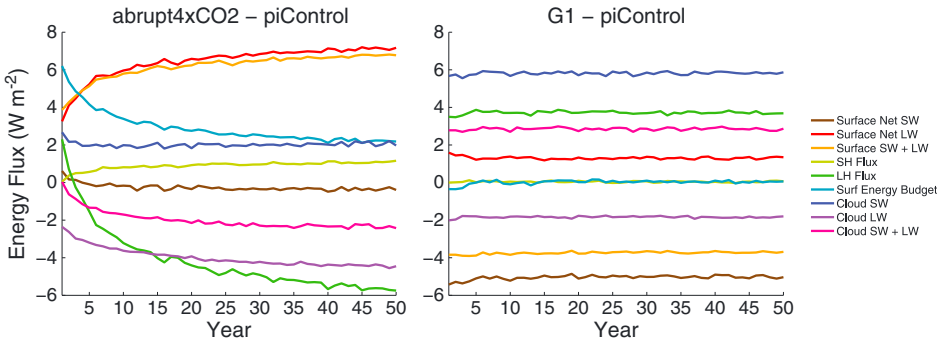

Figure 1. Global averages of surface radiative fluxes for the all-model ensemble mean. SW denotes shortwave radiative flux, LW denotes longwave radiative flux, SH denotes sensible heat flux, LH denotes latent heat flux, and "Surf Energy Budget" denotes the sum SW + LW + SH + LH, which is the right side of equation (1). Cloud forcing is defined as all-sky minus clear-sky radiative fluxes. All fluxes are positive in the downward direction.

changes in surface turbulent heat fluxes, i.e., sensible and latent heat fluxes [*Boer*, 1993]. More specifically,

$$\rho h c_p \frac{\mathrm{d}T}{\mathrm{d}t} = \mathrm{SW} + \mathrm{LW} + \mathrm{SH} + \mathrm{LH} \tag{1}$$

where ρ denotes the density of the medium (kg m^{-3}), h denotes a length scale associated with ocean heat uptake (m), c_p denotes the specific heat of the surface (W m^{-2} K^{-1}), T is temperature (K), t is time (s), SW is shortwave radiation (W m^{-2}), LW is longwave radiation (W m^{-2}), SH is sensible heat flux (W m^{-2}), and LH is latent heat flux (W m^{-2}). These abbreviations are consistent throughout the remainder of this paper.

[19] Section 4.1 contains analyses of changes in radiative fluxes, i.e., shortwave and longwave radiative fluxes, which induce changes in sensible and latent heat fluxes. Section 4.2 shows analyses of the resulting changes in sensible and latent heat fluxes, which indicate changes in evaporative moisture flux, as well as land-sea contrast of temperature and moisture changes. Section 4.3 includes an evaluation of changes in the right side of equation (1), which gives an indication of heat storage, mostly via ocean heat uptake.

4.1. Surface Radiative Fluxes

[20] A change in solar irradiance, as in *G1*, has qualitatively different radiative effects than a change in CO_2 concentrations. An increase in CO_2 primarily affects longwave radiation in the free troposphere. In contrast, although some amount of solar irradiance is absorbed in the free troposphere, most passes through the atmosphere; hence, the primary effects of a solar irradiance reduction are at the surface [e.g., *Bala et al.*, 2010]. The climate response shown for experiment *G1* is a combination of forcing from CO_2 and solar reduction. As such, the results of *abrupt4xCO2* can be used to characterize the CO_2-driven parts of the response in *G1*. Figure 1 shows globally averaged changes in radiative fluxes, including shortwave, longwave, and total surface radiative fluxes. Figure 2 shows model spread for global, land, and ocean averages of changes in surface radiative fluxes. Figure 3 shows the spatial distribution of the rapid adjustment for these three radiative fluxes, and Figure S1 shows the feedback response.

[21] The rapid adjustment of *abrupt4xCO2* shows a small globally averaged net shortwave radiative flux increase due to a number of contributing factors, although model agreement on the locations of these changes is not robust (Figure 3). An increase in CO_2 concentrations increases atmospheric absorption of solar irradiance in the solar CO_2 absorption band, reducing received shortwave radiative flux at the surface. However, this effect is surpassed by an increase in net shortwave radiative flux due to cloud forcing (Figure 4; *cloud forcing* is defined as all-sky minus clear-sky changes in radiative fluxes), which is in part indicative of reduced cloud cover resulting from tropospheric adjustment and increased stability [*Andrews and Forster*, 2008; *Gregory and Webb*, 2008; *Andrews et al.*, 2009]. In the feedback response (Figure S1), net shortwave radiative flux decreases throughout most of the tropics and midlatitudes, indicating a relaxation of the rapid adjustment (Figure 1). Part of this decrease is due to increased absorption of shortwave radiation by the atmosphere, a consequence of increased tropospheric water vapor, which is described by the Clausius-Clapeyron relation (Figure 5). The Arctic shows a further increase in net shortwave radiative flux in the feedback response (Figure S1), which is consistent with continued melting of sea ice [*Kravitz et al.*, 2013]; this is one of the few large-scale robust features of the shortwave feedback response of *abrupt4xCO2*.

[22] The rapid adjustment of *G1* shows a decrease in shortwave radiative flux at the surface, consistent with a reduction in solar irradiance (Figure 2). This decrease shows latitudinal dependence (Figure 3), consistent with a uniform solar reduction [e.g., *Govindasamy and Caldeira*, 2000]. Globally averaged shortwave cloud forcing increases; the cloud forcing in *G1* is approximately twice the forcing in *abrupt4xCO2* (Figure 2). Any changes in cloud cover that would result in increases in shortwave cloud forcing are due to a combination of tropospheric radiative adjustment to increased CO_2 concentrations [*Andrews et al.*, 2009] and increases in atmospheric stability [*Bala et al.*, 2008; *Kravitz et al.*, 2013]. However, some of these apparent changes are due to cloud masking of clear-sky radiative fluxes [*Andrews et al.*, 2009]. That is, due to the reduction of solar irradiance in *G1*, changes in surface shortwave radiative fluxes will be larger in clear-sky than in all-sky, which will generate an apparent large positive shortwave

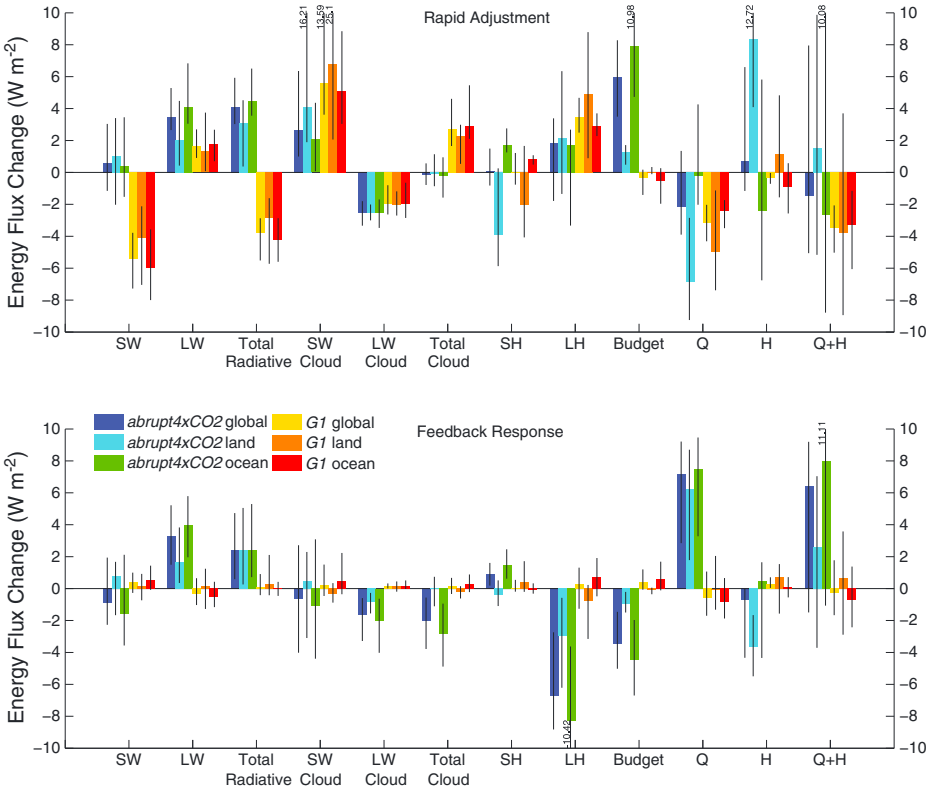

Figure 2. Bar chart showing the rapid adjustment (year 1 average) and feedback response (years 11–50 average minus year 1 average) for radiative flux differences from *piControl*. Colored bars indicate the all-model ensemble mean (Table S1), and black lines indicate the range of model response. Numbers located next to black lines, where displayed, indicate the maximum value of the bar when outside of the chosen range of the axes. Cloud forcing is defined as all-sky minus clear-sky radiative fluxes.

cloud forcing when taking the difference between these two quantities. Because temperature changes in *G1* are small, the feedback response is small (Figures 1 and 2). Changes in the feedback response of shortwave radiative flux are negligible, with few robust features (Figure S1). The results presented here are consistent with those of *Schmidt et al*. [2012].

[23] These changes in downward longwave radiative flux are attributable to specific changes in atmospheric constituents. The dominant contributors to this flux are changes in cloud fraction and changes in emissivity. Contributions from clouds (Figures 4 and S2) can be calculated as all-sky minus clear-sky, although analysis of this quantity will also be contaminated by cloud masking. That is, forcing from emissivity changes is larger in clear-sky than all-sky conditions because optically thick clouds mask part of the radiative effects of emissivity changes. The contribution from emissivity can be further divided into changes in noncondensing greenhouse gases (in these simulations, CO_2), which have a ubiquitous forcing in the models, and changes in temperature and condensing greenhouse gases (primarily water vapor). The Clausius-Clapeyron relation [e.g., *Schneider et al*., 2010] indicates that changes in temperature and changes in water vapor are difficult to separate from each other, but the combination of these two effects can be separated from the effects of the noncondensing gases.

[24] Following the discussion of *Wang and Liang* [2009],

$$L_{\mathrm{dc}} = \varepsilon \sigma T^4 \tag{2}$$

where L_{dc} is the clear sky downward longwave radiative flux at the surface, ε is the emissivity of the atmosphere, $\sigma = 5.67 \times 10^{-8}$ W m^{-2} K^{-4} is the Stefan-Boltzmann constant, and T is the emission temperature of the atmosphere radiating as a blackbody. We can also write

$$L_d = (1-f)L_{\mathrm{dc}} + f\sigma T^4 \tag{3}$$

where L_d is the all-sky downward longwave radiative flux at the surface and f is cloud fraction. Because the models output the longwave radiative fluxes at the surface, we can solve for ε, obtaining

$$\varepsilon = \frac{L_{\mathrm{dc}} f}{L_d - (1-f)L_{\mathrm{dc}}} \tag{4}$$

[25] Figure 6 shows plots of changes in ε for *abrupt4xCO2* and *G1*. In *abrupt4xCO2*, the rapid adjustment increase in Antarctic emissivity is 0.06, and in *G1* is 0.02, compared to a baseline value of 0.37 in *piControl*. This region was chosen because it has the smallest increase in water vapor (Figure 5), although comparing these two values clearly indicates that some amount of water vapor has entered the Antarctic in

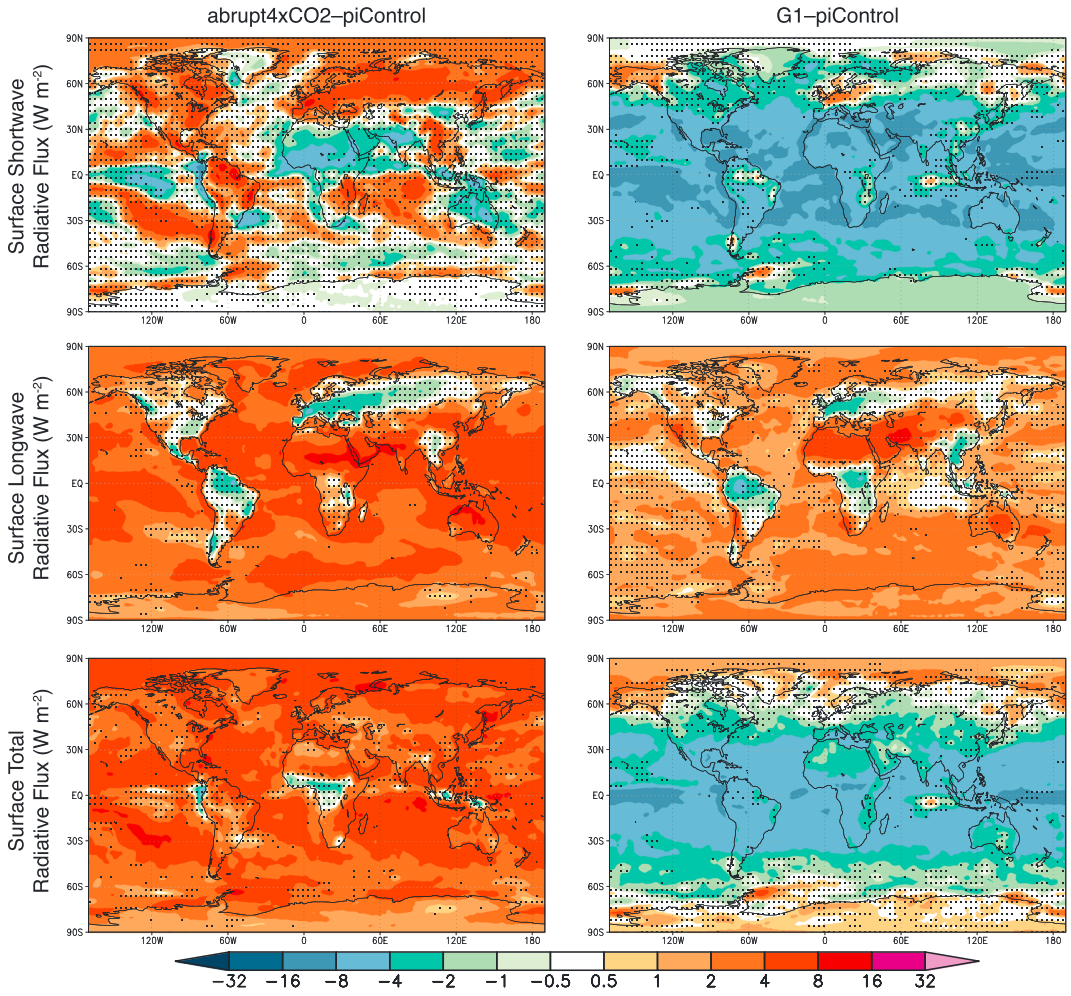

Figure 3. Rapid adjustment of surface shortwave, longwave, and total (shortwave plus longwave) radiative flux differences (W m^{-2}) for the all-model ensemble mean. All values shown are averages over year 1 of the simulation, with positive values indicating increases in the downward direction. Stippling denotes where fewer than 75% of models (8 out of 11) agreed on the sign of the difference.

the *abrupt4xCO2* simulation. The tropical increase in emissivity in the *abrupt4xCO2* feedback response (Figure 6), as well as the increase in downward longwave radiative flux (Figure S1), correlates well with the increase in tropical water vapor (Figure 5). This allows us to conclude that although increases in emissivity due to CO_2 are nonnegligible, the dominant reason for an increase in clear-sky downward longwave radiative flux in *abrupt4xCO2* is an increase in water vapor. Because temperatures do not increase in *G1*, by the Clausius-Clapeyron relation, atmospheric water vapor should not show large changes, whereas it should increase substantially in *abrupt4xCO2*. Due to the latitudinally varying reduction in shortwave radiation, the tropics show cooling in *G1* [*Kravitz et al.*, 2013], which results in reduced tropical water vapor (Figure 5). For these reasons, *G1* shows much smaller rapid adjustment changes in emissivity than *abrupt4xCO2*, and in regions that do not show changes in water vapor, indicating that CO_2 plays a more important role in increasing longwave radiative flux than changes in water vapor. Regions with a strong net cloud forcing (Figure 4) show small changes in emissivity for both *abrupt4xCO2* and *G1*, indicating the effectiveness of clouds in masking longwave increases due to CO_2 or water vapor.

[26] For *abrupt4xCO2*, the net rapid adjustment of total (shortwave + longwave) radiative flux shows a nearly ubiquitous increase, primarily due to longwave radiative flux increases (Figure 3). The feedback response shows a further increase, also primarily due to the longwave response. The rapid adjustment of net cloud forcing is small, whereas the feedback response is a net decrease in cloud forcing, predominantly due to the longwave effect.

[27] For *G1*, the rapid adjustment of globally averaged total radiative flux is negative (Figure 2); the decrease in solar irradiance has a stronger effect on the surface than the increase in longwave radiative flux. The net rapid adjustment of cloud forcing is positive, particularly in the tropics (Figure S1), which is overwhelmingly due to the shortwave effect. The net radiative effect in the Arctic is slightly positive, which is consistent with the results of *Kravitz et al.* [2013], who showed slight reductions in Arctic sea ice (all-model ensemble mean) in *G1*. As discussed previously, the feedback response in *G1* is small, with few robust features.

[28] The latitudinal dependence of cloud forcing is seen in both the shortwave and total radiative flux fast response of *G1* (Figure S1), although some of the apparent cloud forcing

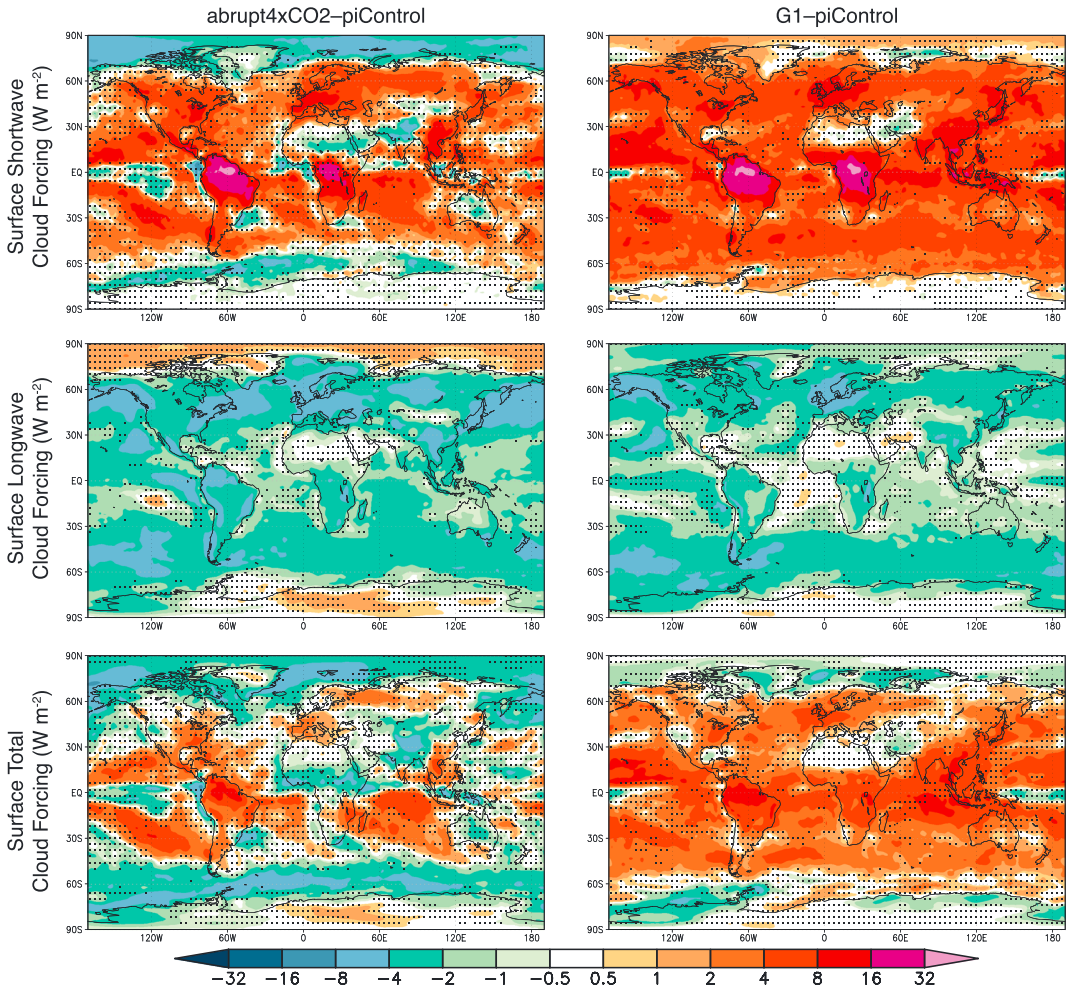

Figure 4. Rapid adjustment of cloud shortwave, longwave, and total (shortwave plus longwave) forcing differences for the all-model ensemble mean. Cloud forcing is calculated as the difference between all-sky and clear-sky conditions. All quantities shown are averages over year 1 of the simulation, with positive values indicating increases in the downward direction. Stippling denotes where fewer than 75% of models (7 out of 9) agreed on the sign of the difference.

is likely due to cloud masking, which is described above. Reduced cloud cover in *G1* results in a net positive forcing, meaning solar irradiance must be further reduced to prevent surface air temperature increases. In this sense, the responses of clouds to the reduced solar radiation act as a negative feedback on the radiative effects of solar geoengineering. *Schmidt et al*. [2012] cited cloud adjustments as the reason solar irradiance needed to be reduced in *G1* further than simple energy balance calculations would suggest.

[29] The individual models show comparable qualitative responses for both *abrupt4xCO2* and *G1* in the rapid adjustment and feedback responses for the global average (Figures S7–S9). The land response is significantly more variable, likely in part due to intermodel differences in cloud adjustment, with some models showing opposite rapid adjustments from others, particularly for *abrupt4xCO2*.

4.2. Sensible and Latent Heat Fluxes

[30] The turbulent heat fluxes, i.e., sensible and latent heat fluxes, are induced by shortwave and longwave radiative fluxes. If adjusted radiative forcing is not the same at both the surface and TOA, there will be an induced change in the turbulent components at the surface to maintain the tropospheric heat balance [*Andrews et al*., 2009]. The Bowen ratio is defined as the ratio of sensible to latent heat fluxes, i.e.,

$$B = {}^{\mathrm{SH}}/_{\mathrm{LH}} \tag{5}$$

[31] A decrease in the Bowen ratio indicates that more energy is used to change the phase of water, implying that particular region is becoming wetter. Conversely, an increase in the Bowen ratio implies that a region is becoming dryer. This explanation ignores changes in circulation that may result in changes in moisture advection, but the explanation provided here is true for a global average and explains a significant portion of regional response; the energetic equivalent of moisture advection is revisited in section 5.2. Understanding the climate response to changes in these turbulent fluxes is crucial: *Ban-Weiss et al*. [2011] found that

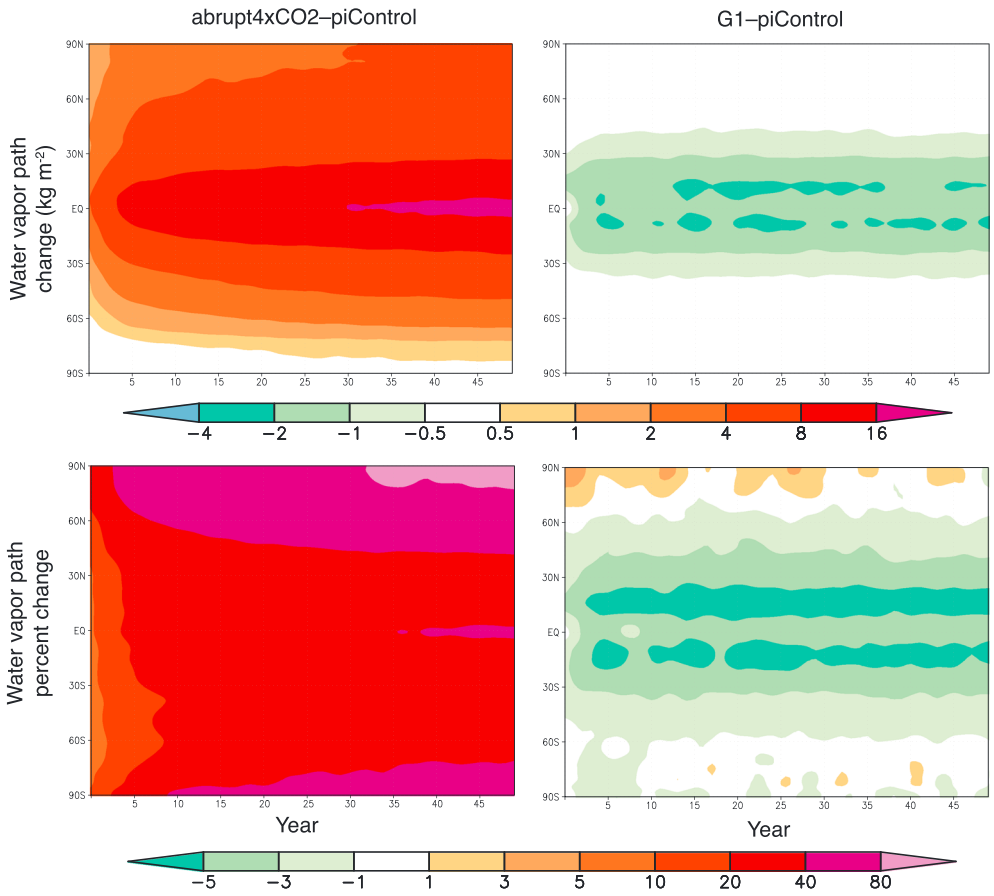

Figure 5. Zonal, annual averages of column-integrated water vapor path for the all-model ensemble mean. Top row shows absolute values (kg m^{-2}), and bottom row shows percent change relative to *piControl*.

simply repartitioning latent and sensible heat fluxes results without changing the net energy content of the climate system results in cloud feedbacks that alter both global and local temperatures. Changes in turbulent fluxes are shown in Figures 1, 2 , 7, S3, and S10–S12. Note that we continue the sign convention adopted previously in the paper, namely that positive values indicate a net flux downward. This convention is the opposite of how turbulent heat fluxes are usually reported, so in this section, descriptions of the direction of the flux are provided wherever possible.

[32] The rapid adjustment of sensible heat flux in *abrupt4xCO2* shows an increased net flux from the land surface to the atmosphere and a decreased net flux from the ocean surface to the atmosphere (per the chosen sign convention, net sensible heat flux decreases over land and increases over oceans). In the feedback response, net sensible heat flux from the surface to the atmosphere is reduced, predominantly over the ocean. The rapid adjustment of net latent heat flux is a net flux from the atmosphere to the surface over both land and ocean; in the feedback response, this pattern is reversed. This results in a rapid adjustment increase in the Bowen ratio over land, but a decrease over ocean and in the global average; the feedback response shows a decrease over the ocean and no change over land.

[33] The responses of the turbulent fluxes in *abrupt4xCO2* are consistent with other studies [e.g., *Ramanathan*, 1981; *O'Gorman and Schneider*, 2008; *Liepert and Previdi*, 2009; *Bala et al.*, 2010]. The atmosphere adjusts to an abrupt increase in CO_2 concentrations by reducing condensational heating to maintain radiative-convective equilibrium; radiative flux changes due to CO_2 are greater at TOA than at the surface [*Andrews et al.*, 2009]. Thus, there must be a reduced turbulent flux from the surface to the atmosphere to compensate for this energy imbalance. Over oceans, the abundance of water means nearly all adjustment is via latent heat fluxes, whereas over land, some adjustment is through sensible heat fluxes [*Sutton et al.*, 2007; *Dong et al.*, 2009]. Thus, the expected rapid adjustment to an abrupt increase in CO_2 concentrations is a net reduction in sensible and latent heat fluxes from the surface to the atmosphere. This explanation is overly simple, in that it ignores feedbacks and complicated near-surface effects, including the CO_2 physiological effect discussed below [*Joshi et al.*, 2008; *Andrews et al.*, 2009], but it explains the broad features of the rapid adjustment in *abrupt4xCO2*, as well as part of the reason for the land-sea contrast in turbulent fluxes and temperature change. Over time, the atmosphere warms, and the feedback response is an increased net latent heat flux from the surface to the atmosphere and a decreased net sensible heat flux from the surface to the atmosphere [*Dong et al.*, 2009].

[34] In *G1*, the rapid adjustment of sensible heat flux shows the same patterns of change as *abrupt4xCO2*, although with reduced magnitude. The rapid adjustment of latent heat flux shows an increase of approximately a factor of 2 larger than

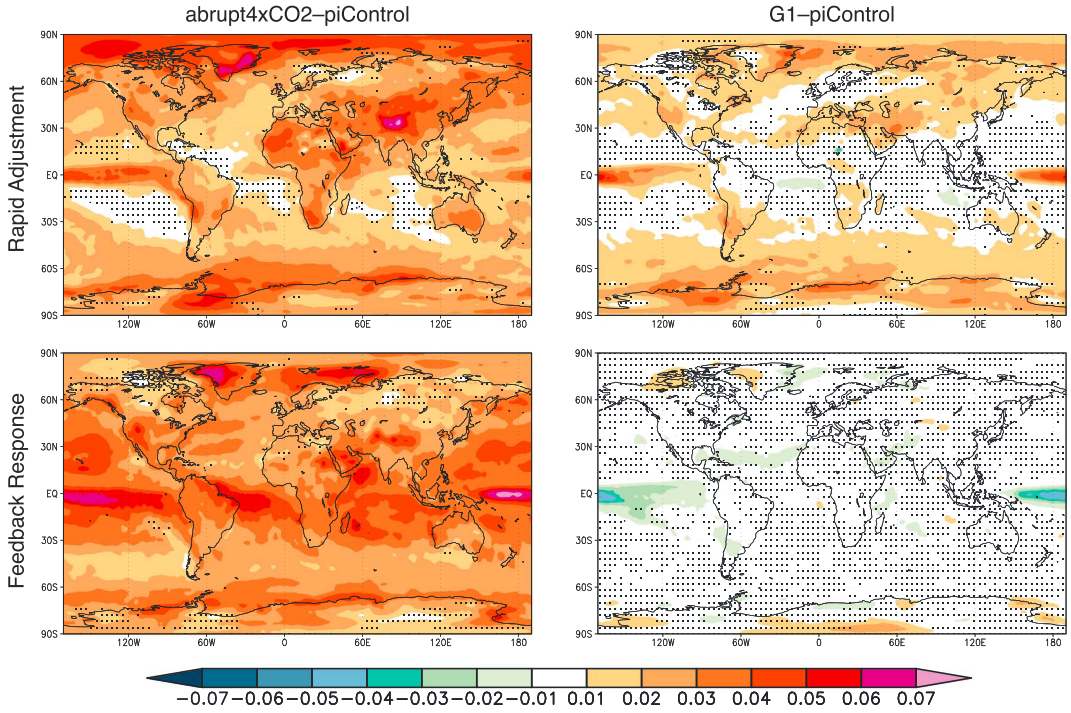

Figure 6. Changes in emissivity (equation (4)) for the all-model ensemble mean. Rapid adjustment indicates averages over year 1 of the simulation, and feedback response indicates a difference between the years 11–50 average and the year 1 average. Stippling denotes where fewer than 75% of models (5 out of 6) agreed on the sign of the difference.

for *abrupt4xCO2*. This results in an increase in the Bowen ratio over land, and a slight decrease over the ocean. As before, small temperature changes in *G1* result in a small feedback response with few robust features (Figures S2 and S3).

[35] Changes in solar irradiance are primarily felt at the surface, whereas the rapid adjustment due to greenhouse gases manifests throughout the free troposphere [*Liepert and Previdi*, 2009]. Because surface temperatures do not change appreciably in *G1*, sensible heat changes are small, so the bulk of the rapid adjustment to the radiative forcing and cloud forcing must therefore be via a strongly reduced net latent heat flux from the surface to the atmosphere. The feedback response is suppressed in *G1*, so this increase in downward longwave radiative flux is maintained, as is the negligible change in sensible heat flux. These results are consistent with the rapid adjustments found by *Bala et al*. [2008] and *Cao et al*. [2012].

[36] Model responses of sensible and latent heat flux are similar to each other, and experiments *abrupt4xCO2* and *G1* show consistently different results (Figures S10–S12). In particular, most models show a rapid adjustment decrease in terrestrial sensible heat flux (i.e., increase in terrestrial net heat flux from the surface to the atmosphere) in the tropics and midlatitudes and a near-uniform increase in oceanic heat flux (less net heat flux from the surface to the atmosphere). Models disagree over the magnitude of the tropical terrestrial sensible heat flux response, with equatorial model response ranging between −20 and 5 W m^{-2} for both *abrupt4xCO2* and *G1*. The rapid adjustment of terrestrial latent heat flux shows an increase (less net heat flux from the surface to the atmosphere) at nearly all latitudes in both *abrupt4xCO2* and *G1*, particularly in the tropics. The increase in equatorial latent heat flux in both experiments ranges between 0 and 35 W m^{-2}. The wide variation in changes can in part be attributed to different land surface parameterizations which affect the strengths of the induced turbulent fluxes.

[37] The changes in sensible heat flux described above are likely specific to this experiment, as the sign of the change in sensible heat is dependent upon the optical thickness of atmospheric longwave absorbers [*O'Gorman and Schneider*, 2008]. However, this will not significantly alter the magnitude of the sensible heat fluxes, and because changes in sensible heat flux are small compared to changes in latent heat flux, we do not expect the qualitative features of our results to be strongly dependent upon experiment design.

[38] In response to rapid increases in CO_2 concentrations, plants close their stomata, reducing evapotranspiration and thus latent heat flux from the surface to the atmosphere; there is an associated increase in net sensible heat flux from the surface to the atmosphere to compensate [e.g., *Field et al*., 1995; *Sellers et al*., 1996; *Dong et al*., 2009]. This effect, known as the CO_2 physiological effect, has been shown to have a significant influence on the rapid adjustment of the land surface energy budget to increased greenhouse gas concentrations, as in *abrupt4xCO2* [e.g., *Naik et al*., 2003; *Cao et al*., 2010; *Andrews et al*., 2011; *Cao et al*., 2012; *Fyfe et al*., 2013]. As this effect is predominantly due to CO_2, effects of a similar magnitude should also be present in *G1* [*Matthews and Caldeira*, 2007].

[39] *Tilmes et al*. [2013] investigated the strength of the physiological effect in one model participating in GeoMIP, Community Climate System Model version 4. They found that the physiological response to *G1* is qualitatively the same as for *abrupt4xCO2*, namely, that evapotranspiration

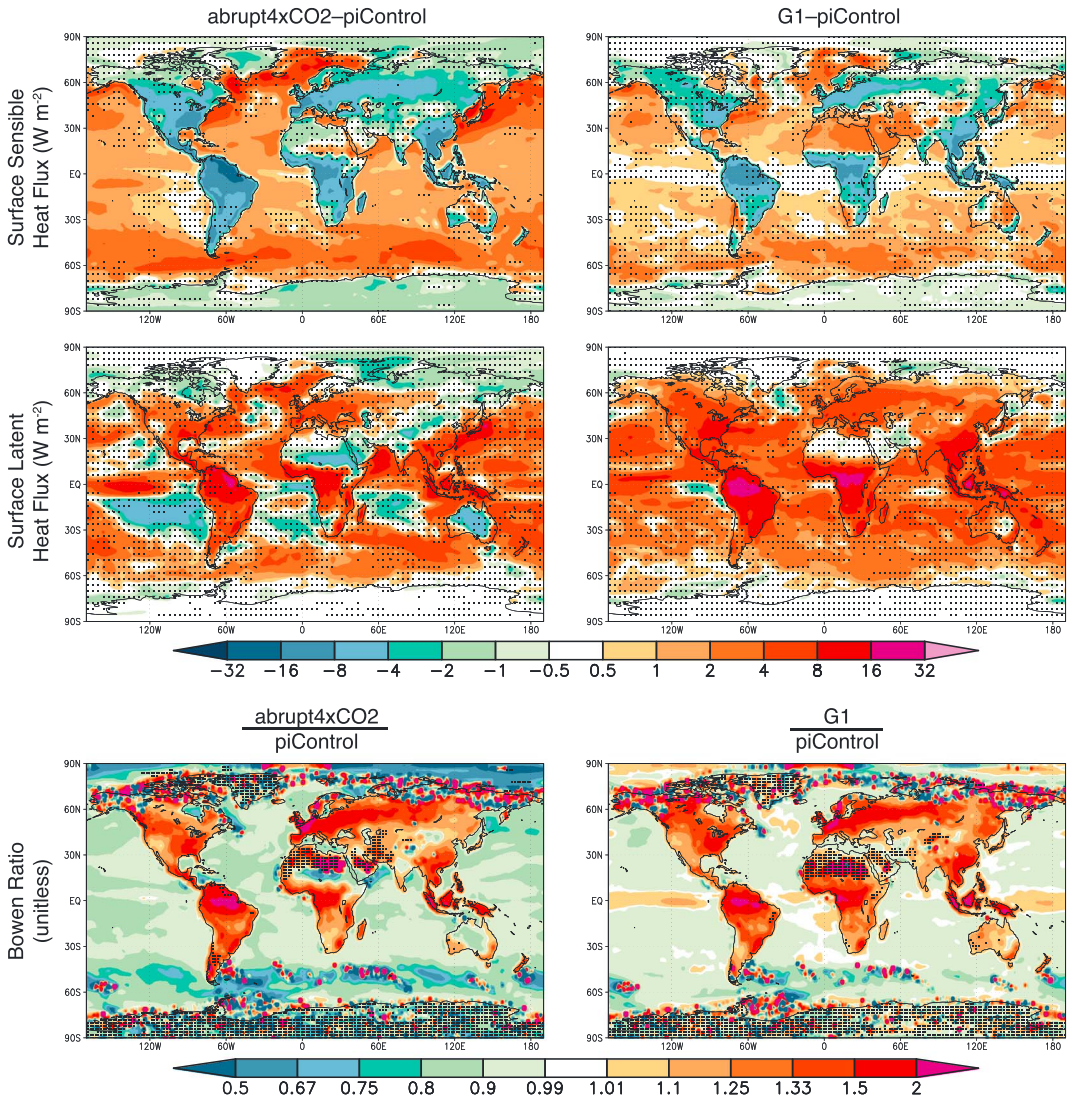

Figure 7. Rapid adjustments of sensible heat flux (W m^{-2}, difference), latent heat flux (W m^{-2}, difference), and Bowen ratio (unitless, ratio) changes for the all-model ensemble mean. All quantities shown are averages over year 1 of the simulation, with positive values indicating increases in the downward direction. The Bowen ratio is defined as the ratio of sensible heat flux to latent heat flux. Stippling denotes (top and middle) where fewer than 75% of models (8 out of 11) agreed on the sign of the difference or (bottom) where fewer than 75% of models agreed whether the ratio of the changes was greater than or less than 1.

decreases, and there is a reduced net latent heat flux from the surface to the atmosphere, while there is an increased net sensible heat flux from the surface to the atmosphere, and hence, land temperatures increase. These results support the conclusions of *Fyfe et al*. [2013] that the CO_2 physiological effect is of similar importance to the radiative effects in determining land turbulent fluxes for geoengineering experiments. However, no other model has conducted GeoMIP-specific simulations which only differ by inclusion of the CO_2 physiological effect, so robust multimodel conclusions cannot be drawn.

[40] All models except EC-Earth include this CO_2 physiological effect [*Kravitz et al*., 2013; *Tilmes et al*., 2013]. Figure S11 reveals that EC-Earth has a small rapid adjustment of land sensible heat flux for both *abrupt4xCO2* and *G1*, whereas all other models show a net sensible heat flux from the surface to the atmosphere, consistent with past studies. Similarly, EC-Earth shows few changes in land latent heat flux, whereas all other models show a reduced net latent heat flux from the surface to the atmosphere in both *abrupt4xCO2* and *G1*, consistent with a reduction in evapotranspiration. Combining these two changes, the Bowen ratio expectedly increases for all models except EC-Earth, predominantly in the tropics.

[41] Due to the high uncertainty in the parameterizations of the CO_2 physiological effect, we are unable to assess the realism of the models' land surface responses in *abrupt4xCO2* and *G1*. As such, these results cannot conclusively determine robust features of the physiological responses to both *abrupt4xCO2* and *G1*. However, they do suggest that this effect is one of the driving forces behind the land-sea contrast in modeled turbulent fluxes. *Fyfe et al*.

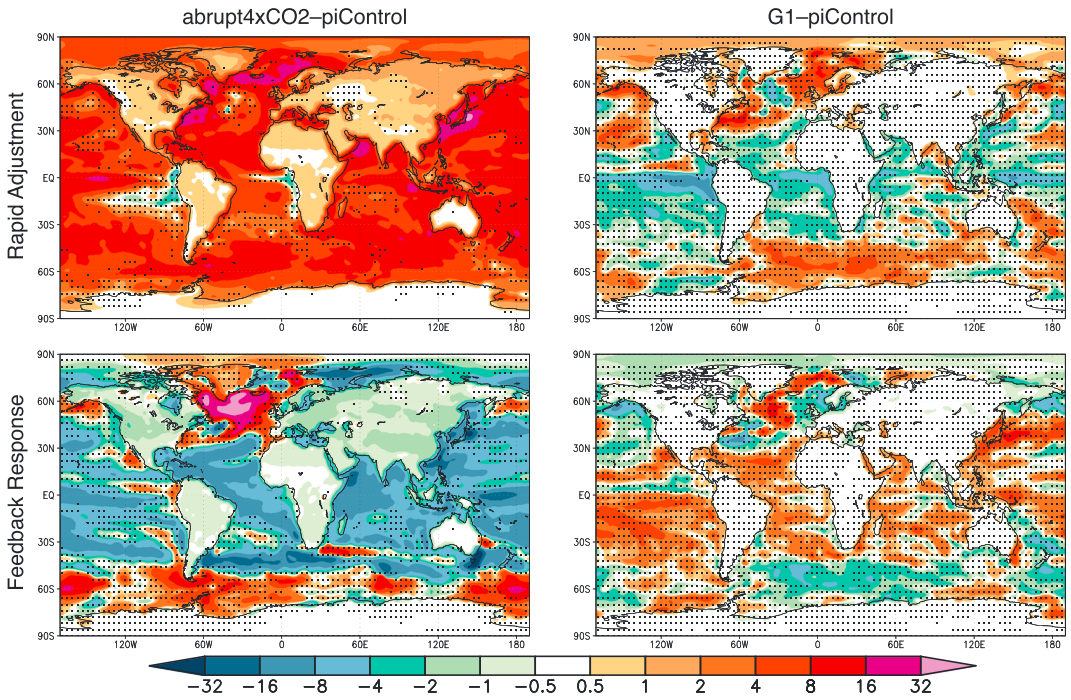

Figure 8. Calculated surface energy budget for the all-model ensemble mean, defined as the sum of net shortwave radiative flux, net longwave radiative flux, sensible heat flux, and latent heat flux. Values are given in W m^{-2}. Rapid adjustment indicates averages over year 1 of the simulation, and the feedback response indicates a difference between year 11–50 averages and year 1 averages. All positive values indicate increases in the downward direction. Stippling denotes where fewer than 75% of models (8 out of 11) agreed on the sign of the difference.

[2013] found different effects for stratospheric sulfate aerosol geoengineering, in part due to an increase in diffuse solar irradiance; as such, these results may depend upon the experimental design.

4.3. Surface Energy Balance

[42] The lines in Figure 1 labeled "Surf Energy Budget" and the bars in Figure 2 labeled "Budget" are plots of the sum of changes in shortwave radiative fluxes, longwave radiative fluxes, sensible heat fluxes, and latent heat fluxes (i.e., the right side of equation (1)). This quantity determines how well the surface and atmospheric energy budgets are in balance; when this quantity is nonzero, the surface heat content changes [*Boer*, 1993].

[43] *abrupt4xCO2* shows a globally averaged rapid adjustment of the sum of these radiative fluxes to be 5.99 (3.49 to 8.28) W m^{-2}, and the feedback response to be −3.45 (−5.02 to −1.46) W m^{-2}. This indicates heat uptake over the entire length of the simulation, but at a decreasing rate due to increased tropospheric temperatures and thus increased emission of radiation to space. Conversely, *G1* shows a globally averaged rapid adjustment of −0.35 (−1.41 to 0.17) W m^{-2} and a feedback response of 0.40 (−0.07 to 1.20) W m^{-2}, indicating an initial small loss of heat from the surface in the first year of simulation, followed by virtually no change (the net effect in the years 11–50 average is an increase of 0.05 W m^{-2} for the all-model ensemble mean) in surface heat content throughout the remainder of the simulation.

[44] In the feedback response, the ensemble mean response of both *abrupt4xCO2* and *G1* show patterns (Figures 8 and S13) of net surface heat flux that compare well with observed climatologies (not shown) [*Josey et al.*, 1996, 1999]. Because all of the participating models in this study include fully coupled oceans, a more accurate assessment of ocean heat uptake can be undertaken than in many previous studies that used slab ocean models. In *abrupt4xCO2*, the North Atlantic remains a region of net heat flux from the ocean to the atmosphere, but the flux is reduced by approximately a factor of two; we have not yet ascertained an explanation for this feature. With this exception, nearly the entire ocean shows increased heat uptake. Because *G1* is largely in surface and atmospheric energy balance, there is no indication of large changes in ocean heat uptake in this experiment.

5. Effects of Radiative Changes on the Hydrological Cycle

[45] Because mean precipitation is governed by the availability of energy, specifically the net radiative loss in the free atmosphere, if surface radiative fluxes change, precipitation must change in a way such that the atmospheric energy budget continues to balance [e.g., *Allen and Ingram*, 2002; *O'Gorman et al.*, 2012]. Therefore, the results described in section 4 can be used to explain changes in precipitation in experiments *abrupt4xCO2* and *G1*. This approach, while useful, has limitations, in that there are effects on the hydrological cycle which are not directly determined by the surface

and atmospheric energy budgets. For example, changes in the dynamics of the Hadley circulation and extratropical moisture transport can dampen the precipitation response to global warming [*Held and Soden*, 2006; *Lorenz and DeWeaver*, 2007]. Although we do not analyze these changes, the analysis in section 5.2 below suggests that they can be important for *abrupt4xCO2*, and less so for *G1*.

5.1. Global Changes in Precipitation

[46] Because changes in atmospheric storage of water are relatively small compared to the amount of water that is precipitated and evaporated, changes in globally, annually averaged precipitation are equal to changes in evaporation [*Liepert and Previdi*, 2009; *Wild and Liepert*, 2010]. More specifically, *Liepert and Previdi* [2009] describe long-term precipitation changes via the equation

$$L_c\Delta P = -L_c\Delta E = \Delta\mathrm{LH} = \Delta R_{\mathrm{sfc}} + \Delta\mathrm{SH} - \Delta\mathrm{M} \tag{6}$$

where L_c is the latent heat of condensation of water (approximately 2.5×10^6 W m^{-2} K^{-1}), ΔP is change in precipitation, ΔE is change in evaporation, ΔLH is change in latent heat flux, ΔR_{sfc} is change in surface radiative fluxes (shortwave + longwave), ΔSH is change in sensible heat flux, and ΔM is heat storage by the surface. (Note that this approach neglects effects on heat storage due to changes in snow and ice.) On a decadal time scale, $\Delta M = \Delta R_{\mathrm{TOA}}$ [*Hansen et al*., 2005; *Liepert and Previdi*, 2009]. Substituting this relation, we obtain the formulation of *O'Gorman et al*. [2012]

$$L_c\Delta P = \Delta R_{\mathrm{sfc}} - \Delta R_{\mathrm{TOA}} + \Delta\mathrm{SH} \tag{7}$$

[47] The right side of equation (7) is denoted ΔQ, as is done by *Muller and O'Gorman* [2011], to give

$$\Delta\mathrm{Q} = \Delta R_{\mathrm{sfc}} - \Delta R_{\mathrm{TOA}} + \Delta\mathrm{SH} \tag{8}$$

[48] Q is defined as the column-integrated diabatic cooling (excluding latent heating), which is the energetic equivalent of evaporative moisture flux and is the primary contributor to mean precipitation. This is clear in light of equation (6), although the formulation of equation (8) can be generalized, so it is applicable to both global and local scales, described in section 5.2 below. Maps showing spatial distributions of changes in Q can be found in Figures 9 and S4.

[49] Although the relation $\Delta M = \Delta R_{\mathrm{TOA}}$ applies on a decadal time scale, by definition, ΔM should be small in the rapid adjustment. By experimental design, ΔR_{TOA} is approximately 0 in *G1*, so $\Delta M = \Delta R_{\mathrm{TOA}}$ indeed holds (approximately), meaning equation (7) is applicable to *G1* regardless of time scale. However, in *abrupt4xCO2*, ΔR_{TOA} is positive, so $\Delta M = \Delta R_{\mathrm{TOA}}$ does not hold. Combining equations (6) and (8), the following relationship is obtained: $L_c\Delta P = \Delta Q + \Delta R_{\mathrm{TOA}} - \Delta M$. As such, the change in precipitation in *abrupt4xCO2* should be more positive (increase in precipitation or smaller decrease) than would be indicated by the quantity ΔQ. Below, we explore the effects on the accuracy of ΔQ in predicting the precipitation changes discussed by *Kravitz et al*. [2013] and *Tilmes et al*. [2013].

[50] The rapid adjustment of *abrupt4xCO2* shows a decrease in Q, which is dominated by the land surface response (Figure 2). The feedback response shows an increase that is much larger than the decrease seen in the rapid adjustment. ΔQ has a distinct land-ocean contrast in the sign of the rapid adjustment, but the increase in the feedback response is near uniform.

[51] In *G1*, the rapid adjustment of Q shows an even greater globally averaged decrease than in *abrupt4xCO2*; unlike for *abrupt4xCO2*, the decrease is substantial over both land and ocean. The feedback response shows few changes, consistent with previous statements that temperature-related feedbacks are suppressed. Models generally show agreement on zonal changes in Q in both *abrupt4xCO2* and *G1*, although some models are more responsive than others (Figures S14–S16).

[52] Changes in Q accurately explain the mean precipitation changes found by *Kravitz et al*. [2013] and *Tilmes et al*. [2013]. In these studies, both *abrupt4xCO2* and *G1* show a rapid adjustment of reduced precipitation; while precipitation later increases in *abrupt4xCO2* as a response to temperature increases, it remains suppressed in *G1*. This is in part due to the definition of rapid adjustment adopted in this paper (see section 3). The definition of rapid adjustment chosen for this paper underestimates precipitation adjustment in *abrupt4xCO2* because rapid adjustment to an increase in CO_2 concentrations acts to reduce precipitation, but an increase in temperature increases precipitation [e.g., *Andrews et al*., 2009]. However, in *G1*, changes in temperature are small, so the rapid adjustment of precipitation is reduced even more than in *abrupt4xCO2*, as also discussed by *Tilmes et al*. [2013]. Using a close approximation that 1 mm day^{-1} of precipitation is approximately equivalent to 29 W m^{-2} of energy flux [*Muller and O'Gorman*, 2011], the fast response of *abrupt4xCO2* shows a decrease in global precipitation by 0.07 mm day^{-1}, and *G1* shows a decrease by 0.11 mm day^{-1}; these values are in good agreement with those reported by *Schmidt et al*. [2012] and *Kravitz et al*. [2013]. *Bala et al*. [2008] hypothesized a gradual decrease in the precipitation rate in an experiment similar to *G1*, based on the assumption that the climate response is stabilized, so the surface radiative fluxes are balanced solely by changes in the turbulent fluxes. Our results show no such corresponding feedback response in Q.

[53] In the globally averaged rapid adjustment of *abrupt4xCO2*, $\Delta R_{\mathrm{sfc}} = 4.08$ W m^{-2} (all-model ensemble mean), $\Delta\mathrm{SH} = 0.08$ W m^{-2}, and $\Delta Q = -2.17$ W m^{-2}, meaning $\Delta R_{\mathrm{TOA}} = 6.33$ W m^{-2} by equation (8). Similarly, *G1* shows a rapid adjustment of $\Delta R_{\mathrm{sfc}} = -3.81$ W m^{-2} (all-model ensemble mean), $\Delta\mathrm{SH} = -0.01$ W m^{-2}, and $\Delta Q = -3.14$ W m^{-2}, so $\Delta R_{\mathrm{TOA}} = -0.68$ W m^{-2}; this last value is consistent with values reported by *Kravitz et al*. [2013]. These values are consistent with the explanation by *O'Gorman et al*. [2012] that if radiative fluxes change, precipitation must change in such a way as to balance the total column atmospheric energy budget. The value of ΔQ effectively determines the amount of adjustment by precipitation to account for average column energy imbalances. ΔQ is greater in the rapid adjustment of *G1* than *abrupt4xCO2*. As such, precipitation reductions in the rapid adjustment of *G1* should be greater in magnitude than in the fast response of *abrupt4xCO2*.

[54] Figure S1 of *Kravitz et al*. [2013] shows that the precipitation reduction in the first year is greater for *G1* than for *abrupt4xCO2*, consistent with the reported values of ΔQ. Using the regression method discussed in section 3, *Tilmes*

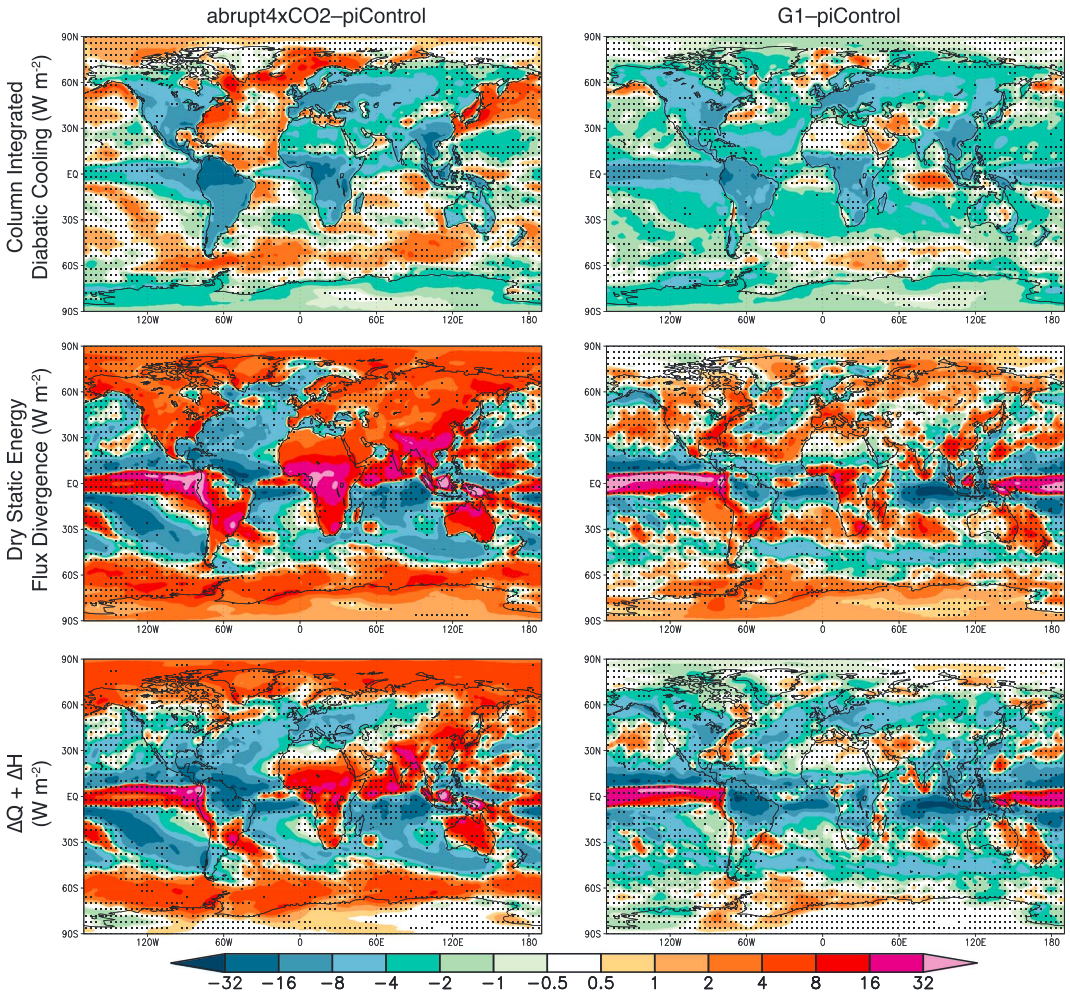

Figure 9. Rapid adjustment of column-integrated diabatic cooling (Q), dry static energy flux divergence (H), and the sum of the two quantities for the all-model ensemble mean. All quantities shown are averages over year 1 of the simulation, with positive values indicating increases in the downward direction. Stippling denotes where fewer than 75% of models (8 out of 11) agreed on the sign of the difference.

et al. [2013] found that the regressed precipitation reduction in *G1* is less than for *abrupt4xCO2*. The discrepancy between calculations of these two methods is in part due to the fact that averages over the first year of simulation already include some amount of warming in *abrupt4xCO2*, explaining why the rapid adjustment of Q reported in this paper is greater for *G1* than *abrupt4xCO2*.

[55] The results presented here are consistent with explanations invoking change in moist static stability. The definition of rapid adjustment is that tropospheric temperatures adjust before ocean temperatures have time to change [*Gregory and Webb*, 2008]. This reduces convective precipitation by increasing atmospheric stability [*Dong et al*., 2009; *Bony et al*., 2013], causing a rapid adjustment of reduced precipitation and evaporation [*Bala et al*., 2010]. As temperatures increase due to increased CO_2, both surface and tropospheric temperatures increase; this maintains a moist adiabatic lapse rate, so precipitation increases [*Lambert and Webb*, 2008]. However, because solar reduction affects the surface more than the troposphere, the atmospheric lapse rate decreases, and moist static stability increases [*Bala et al*., 2008; *Kravitz et al*., 2013].

[56] The long-term global average of precipitation minus evaporation ($P-E$) should be 0. This relationship should also hold for the energetic equivalents of these quantities, namely that $\Delta Q + \Delta \mathrm{LH}$ should also be 0. (Because all net radiative fluxes are defined as positive downward, we take the sum of Q and LH instead of the difference.) The globally averaged rapid adjustment of $Q + \mathrm{LH}$ for *abrupt4xCO2* is -0.34 W m^{-2}, and the feedback response is 0.39 W m^{-2}. For *G1*, the rapid adjustment flux is $Q + \mathrm{LH}$ is 0.32 W m^{-2}, and the feedback response is -0.32 W m^{-2}. These results are consistent with *Kravitz et al*. [2013], who found that globally averaged $P-E$ remains largely unchanged in *G1*, even though both P and E are reduced, resulting in a weaker hydrological cycle [*Tilmes et al*., 2013].

5.2. Local Changes in Precipitation

[57] In the global, long-term average, precipitation and evaporation rates are equal. Locally, the precipitation rate is the sum of contributions from evaporation and moisture convergence. *Muller and O'Gorman* [2011] describe these two contributory quantities in terms of energetics. One quantity is the column-integrated diabatic cooling (excluding

latent heating), introduced above as Q. The second quantity, denoted H by *Muller and O'Gorman* [2011], is the dry static energy flux divergence associated with the circulation, which is the energetic equivalent of moisture convergence. This quantity is defined by

$$L_c\Delta P = \Delta Q + \Delta H \tag{9}$$

[58] Changes in Q can explain mean changes in precipitation, as was shown in section 5.1, but describing spatial variability of precipitation changes also requires discussions of changes in H. Maps showing changes in spatial distributions of both Q and H can be found in Figures 9 and S4.

[59] Similarly to ΔQ, the rapid adjustment of H in *abrupt4xCO2* shows a distinct land-sea contrast (Figure 2); H increases over land and decreases over ocean, with a slight increase in the global mean. The feedback response shows a slight global decrease in H, primarily due to a decrease over land. ΔH in both the rapid adjustment and feedback responses shows strong, robust increases (>32 W m^{-2}) in parts of the Intertropical Convergence Zone (ITCZ), which is consistent with reduced tropical stability and increased convective precipitation [*Kravitz et al*., 2013; *Tilmes et al*., 2013].

[60] The rapid adjustment of H in *G1* shows a slight globally averaged decrease with little robustness. There is some increase in ΔH in the ITCZ that is compensated by a decrease in ΔQ in this region. The feedback response shows few changes. Figures S14–S16 show that model behavior of H is highly variable in both *abrupt4xCO2* and *G1*.

[61] The sum of these quantities, which is L_cP by equation (9), shows an overall rapid adjustment decrease in *abrupt4xCO2*. In the land average, the rapid adjustment in *abrupt4xCO2* is $\Delta Q + \Delta H = 1.52$ W m^{-2}, indicating an increase in land precipitation, despite a decrease in total precipitation; these results are consistent with those of *Kravitz et al*. [2013]. These results are also quite similar to those found by *Cao et al*. [2012], who found that the causes for the precipitation and evaporation changes in *abrupt4xCO2* are manifest within days. In *G1*, ΔH is relatively weak, so the rapid adjustment of precipitation is mostly due to changes in Q. Thus, rapid adjustments of precipitation in *abrupt4xCO2* are due to both mean changes in evaporation and changes associated with moisture convergence, with both quantities showing a strong land-sea contrast. Conversely, changes in precipitation in *G1* are largely due to mean changes in evaporation and much less so by circulation changes. *Muller and O'Gorman* [2011] attribute most changes in H as due to changes in the mean circulation (e.g., Hadley, Ferrel, and Walker cells). Thus, our results suggest that changes in the annual mean circulation are small in *G1*, although changes on a seasonal time scale could still be important. This is consistent with the perspective that the rapid adjustment of *abrupt4xCO2* will have a land warming component, which would likely cause changes in circulation, but this land warming is partially offset in *G1*, implying fewer circulation changes. Indeed, the all-model ensemble mean rapid adjustment shows land warming of 1.91 K for *abrupt4xCO2* and 0.43 K for *G1*. However, analyses of circulation changes are beyond the scope of this work.

[62] In the global mean, $\Delta Q + \Delta\mathrm{LH}$ is small, indicating that global changes in $P-E$ are also small in *G1*. Figures S5 and S6 attempt to discern whether a similar relationship holds on a local scale. The rapid adjustment of $\Delta Q + \Delta\mathrm{LH}$ shows robust decreases over land regions, and $\Delta H + \Delta\mathrm{LH}$ shows robust increases over land regions, but these findings are dominated by the changes in Q and H, which are large compared to changes in latent heat flux. Overall, there is no indication that $\Delta Q + \Delta H$ is equal to changes in latent heat flux on a local scale, indicating that *abrupt4xCO2* shows large local changes in $P-E$; this result was also found by *Kravitz et al*. [2013] (also consistent with *Tilmes et al*. [2013, Figure 3]). Conversely, the rapid adjustment of *G1* shows that $\Delta Q + \Delta H + \Delta\mathrm{LH}$ is 0.10 W m^{-2} in the global average. In the land average, $\Delta Q + \Delta\mathrm{LH} = -0.06$ W m^{-2}, but $\Delta H = 1.15$ W m^{-2}, indicating that circulation changes positively contribute to precipitation changes over land, although less than for *abrupt4xCO2*. Over the ocean, $\Delta Q + \Delta H + \Delta\mathrm{LH} = -0.45$ W m^{-2}, with ΔQ and ΔH both contributing negatively to precipitation.

6. Discussion and Conclusions

[63] Our study is the first intercomparison of fully coupled atmosphere-ocean general circulation models to assess changes in the surface energy budget due to geoengineering. These changes can be used to understand how the atmosphere adjusts to the combination of CO_2 increases and compensating solar reductions, and in turn how precipitation adjusts to these energy flux changes. In particular, use of many models improves confidence in our results. We summarize the main conclusions from our study as follows:

[64] 1. Because temperature increases are suppressed in *G1*, the feedback response in *G1* is small.

[65] 2. The rapid adjustment of *abrupt4xCO2* shows an increase in downward longwave surface radiative flux primarily due to cloud cover changes and increases in water vapor. The increase in downward longwave surface radiative flux in *G1* is primarily due to CO_2.

[66] 3. Both *abrupt4xCO2* and *G1* show a rapid adjustment decrease in land sensible heat flux (more net heat flux from the surface to the atmosphere) and an increase in latent heat flux (reduced net heat flux from the surface to the atmosphere). However, *abrupt4xCO2* shows more decrease in sensible heat flux and less increase in latent heat flux, suggesting that the rapid adjustment of *abrupt4xCO2* includes some amount of land temperature increase and less decrease in evaporation than *G1*.

[67] 4. The CO_2 physiological effect appears to be quite important in determining the rapid adjustment of the turbulent fluxes. However, we are unable to ascertain whether this effect is more important than the radiative effects.

[68] 5. *abrupt4xCO2* shows a significant increase in ocean heat uptake, but *G1* shows little change in ocean heat uptake.

[69] 6. An abrupt increase in CO_2 causes an initial suppression in global precipitation, but the rapid adjustment is associated with changes in circulation patterns, which result in an increase in precipitation over land regions [e.g., *Cao et al*., 2012]. In the feedback response, temperature-related feedbacks increase radiative fluxes at the surface; this change in energy balance results in more precipitation.

[70] 7. A reduction in solar radiation imposed upon this CO_2 increase causes an initial suppression in precipitation that is sustained throughout experiment *G1* because the feedback response is small. The energetic perspective used here suggests that changes in the annual mean circulation are small in *G1*.

[71] Although the experiments investigated here are highly idealized, they are quite useful in characterizing more general results regarding offsets of CO_2 forcing with reduced shortwave forcing. Changes in surface forcing and precipitation are approximately linear with changes in CO_2 and insolation [*Andrews et al*., 2009; *Andrews and Forster*, 2010; *Schneider et al*., 2010]. Moreover, because transient simulations of CO_2 increases or shortwave radiative flux reductions are effectively convolutions of infinitesimally small abrupt changes [*Good et al*., 2011], our results are applicable to more realistic scenarios. We do note that our results may be quantitatively different for different greenhouse gas profiles and methods of uniform solar geoengineering. Other potential investigations could include dependence of these results on the type of shortwave forcing, e.g., determining differences between solar reductions and sulfate aerosol injections.

[72] *Bony et al*. [2013] obtained similar results to ours for an increase in CO_2, namely that a large part of the tropical precipitation response to CO_2 is a rapid adjustment, independent of surface warming. They concluded that tropical circulation changes under increased CO_2 have a large rapid adjustment component, and thus offsetting global temperature changes, as in *G1*, will not fully compensate for precipitation changes due to CO_2. Although our equation (9) divides the precipitation response into two components that are not quite comparable to the divisions made by *Bony et al*., we arrive at a similar conclusion; the feedback response of $\Delta Q + \Delta H$ in *G1* is small, meaning the long-term precipitation levels are lower than those of *piControl*. Our conclusions show that this precipitation suppression is primarily due to changes in evaporation, although as we stated in section 5, our explanations do not include potential changes in the Hadley circulation and extratropical moisture transport. Further analysis is needed to determine the exact nature of this difference. Although Hadley circulation changes in response to CO_2 forcing have been analyzed [e.g., *Rind and Rossow*, 1984; *Lu et al*., 2007; *Hu and Fu*, 2007; *Johanson and Fu*, 2009], a thorough comparison of the Hadley circulation changes in *abrupt4xCO2* and *G1* would make a nice complement to our work.

[73] One source of uncertainty in our results is due to the CO_2 physiological effect. Although we have evidence to suggest that this effect is important, we did not conduct sufficient simulations to quantify this effect in all participating models. This effect will be stronger in boreal summer, potentially affecting the seasonal cycle of radiation changes and responses to those changes, and seems to also play an important role in summer NH midlatitudes [*Tilmes et al*., 2013]. Moreover, the CO_2 physiological effect promotes land-sea temperature contrasts [*Joshi and Gregory*, 2008; *Cao et al*., 2012; *Tilmes et al*., 2013]; it would be useful to determine the degree to which our findings regarding land-sea contrasts in energy are affected by this process.

[74] The results we present should not be mistaken as advocacy for geoengineering or any particular scheme therein. Although scientific information will be an essential part of the decision making process, it should not be the only consideration in evaluation of geoengineering proposals.

[75] **Acknowledgments.** We thank three anonymous reviewers for their helpful comments in improving the manuscript. We also thank all participants of the Geoengineering Model Intercomparison Project and their model development teams, CLIVAR/WCRP Working Group on Coupled Modeling for endorsing GeoMIP, and the scientists managing the Earth System Grid data nodes who have assisted with making GeoMIP output available. We acknowledge the World Climate Research Programme's Working Group on Coupled Modelling, which is responsible for CMIP, and we thank the climate modeling groups for producing and making available their model output. For CMIP, the U.S. Department of Energy's Program for Climate Model Diagnosis and Intercomparison provides coordinating support and led development of software infrastructure in partnership with the Global Organization for Earth System Science Portals. Ben Kravitz is supported by the Fund for Innovative Climate and Energy Research (FICER). The Pacific Northwest National Laboratory is operated for the U.S. Department of Energy by Battelle Memorial Institute under contract DE-AC05-76RL01830. Simulations performed by Ben Kravitz were supported by the NASA High-End Computing (HEC) Program through the NASA Center for Climate Simulation (NCCS) at Goddard Space Flight Center. Timothy Andrews was supported by the Joint DECC/Defra Met Office Hadley Centre Climate Programme (GA01101). Duoying Ji and John C. Moore thank all members of the BNU-ESM model group, as well as the Center of Information and Network Technology at Beijing Normal University for assistance in publishing the GeoMIP data set. Alan Robock is supported by NSF grants AGS-1157525 and CBET-1240507. Helene Muri was supported by the EuTRACE project, the European Union 7th Framework Programme grant 306395. Jón Egill Kristjánsson, Ulrike Niemeier, and Michael Schulz received funding from the European Union's Seventh Framework Programme (FP7/2007-2013) under grant agreement 226567-IMPLICC. Jón Egill Kristjánsson received support from the Norwegian Research Council's Programme for Supercomputing (NOTUR) through a grant of computing time. Simulations with the IPSL-CM5 model were supported through HPC resources of [CCT/TGCC/CINES/IDRIS] under the allocation 2012-t2012012201 made by GENCI (Grand Equipement National de Calcul Intensif). Duoying Ji and John C. Moore thank all members of the BNU-ESM model group, as well as the Center of Information and Network Technology at Beijing Normal University for assistance in publishing the GeoMIP data set. The National Center for Atmospheric Research is funded by the National Science Foundation. Shingo Watanabe was supported by the Innovative Program of Climate Change Projection for the 21st century, MEXT, Japan. Computer resources for Philip J. Rasch, Balwinder Singh, and Jin-Ho Yoon were provided by the National Energy Research Scientific Computing Center, which is supported by the Office of Science of the U.S. Department of Energy under Contract DE-AC02-05CH11231.

References

Allen, M. R., and W. J. Ingram (2002), Constraints on future changes in climate and the hydrological cycle, *Nature*, *419*, 223–232.

Andrews, T., and P. M. Forster (2008), CO_2 forcing induces semi-direct effects with consequences for climate feedback interpretations, *Geophys. Res. Lett.*, *35*, L04802, doi:10.1029/2007GL032273.

Andrews, T., and P. M. Forster (2010), The transient response of global-mean precipitation to increasing carbon dioxide levels, *Environ. Res. Lett.*, *5*, 025212, doi:10.1088/1748-9326/5/2/025212.

Andrews, T., P. M. Forster, and J. M. Gregory (2009), A surface energy perspective on climate change, *J. Clim.*, *22*, 2557–2570, doi:10.1175/2008JCLI2759.1.

Andrews, T., M. Doutriaux-Boucher, O. Boucher, and P. M. Forster (2011), A regional and global analysis of carbon dioxide physiological forcing and its impact on climate, *Clim. Dyn.*, *36*, 783–792, doi:10.1007/s00382-010-0742-1.

Bala, G., P. B. Duffy, and K. E. Taylor (2008), Impact of geoengineering schemes on the global hydrological cycle, *Proc. Natl. Acad. Sci. U.S.A.*, *105*, 7664–7669, doi:10.1073/pnas.0711648105.

Bala, G., K. Caldeira, and R. Nemani (2010), Fast versus slow response in climate change: Implications for the global hydrological cycle, *Clim. Dyn.*, *35*, 423–434, doi:10.1007/s00382-009-0583-y.

Ban-Weiss, G. A., G. Bala, L. Cao, J. Pongratz, and K. Caldeira (2011), Climate forcing and response to idealized changes in surface latent and sensible heat, *Environ. Res. Lett.*, *6*, 034032, doi:10.1088/1748-9326/6/3/034032.

Boer, G. J. (1993), Climate change and the regulation of the surface moisture and energy budgets, *Clim. Dyn.*, *8*, 225–239.

Bony, S., G. Bellon, D. Klocke, S. Sherwood, S. Fermepin, and S. Denvil (2013), Robust direct effect of carbon dioxide on tropical circulation and regional precipitation, *Nat. Geosci.*, *6*, 447–451, doi:10.1038/ngeo1799.

Cao, L., G. Bala, K. Caldeira, R. Nemani, and G. Ban-Weiss (2010), Importance of carbon dioxide physiological forcing to future climate change, *Proc. Natl. Acad. Sci. U.S.A.*, *107*, 9513–9518, doi:10.1073/pnas.0913000107.

Cao, L., G. Bala, and K. Caldeira (2012), Climate response to changes in atmospheric carbon dioxide and solar irradiance on the time scale of days to weeks, *Environ. Res. Lett.*, *7*, 034015, doi:10.1088/1748-9326/7/3/034015.

Crutzen, P. J. (2006), Albedo enhancement by stratospheric sulfur injections: A contribution to resolve a policy dilemma?, *Clim. Change*, *77*(3–4), 211–220, doi:10.1007/s10584-006-9101-y.

Dong, B., J. M. Gregory, and R. T. Sutton (2009), Understanding land-sea warming contrast in response to increasing greenhouse gases. Part I: Transient adjustment, *J. Clim.*, *22*, 3079–3097, doi:10.1175/2009JCLI2652.1.

Field, C., R. Jackson, and H. Mooney (1995), Stomatal responses to increased CO_2: Implications from the plant to the global scale, *Plant Cell Environ.*, *18*, 1214–1255, doi:10.1111/j.1365-3040.1995.tb00630.x.

Fyfe, J. C., J. N. S. Cole, V. K. Arora, and J. F. Scinocca (2013), Biogeochemical carbon coupling influences global precipitation in geoengineering experiments, *Geophys. Res. Lett.*, *40*, 651–655, doi:10.1002/grl.50166.

Good, P., J. M. Gregory, and J. A. Lowe (2011), A step-response simple climate model to reconstruct and interpret AOGCM projections, *Geophys. Res. Lett.*, *38*, L01703, doi:10.1029/2010GL045208.

Govindasamy, B., and K. Caldeira (2000), Geoengineering Earth's radiation balance to mitigate CO_2-induced climate change, *Geophys. Res. Lett.*, *27*, 2141–2144, doi:10.1029/1999GL006086.

Gregory, J. M., and P. M. Forster (2008), Transient climate response estimated from radiative forcing and observed temperature change, *J. Geophys. Res.*, *113*, D23105, doi:10.1029/2008JD010405.

Gregory, J., and M. Webb (2008), Tropospheric adjustment induces a cloud component in CO_2 forcing, *J. Clim.*, *21*(1), 58–71, doi:10.1175/2007JCLI1834.1.

Gregory, J. M., et al. (2004), A new method for diagnosing radiative forcing and climate sensitivity, *Geophys. Res. Lett.*, *31*, L03205, doi:10.1029/2003GL018747.

Hansen, J., et al. (2005), Earth's energy imbalance: Confirmation and implications, *Science*, *308*, 1431–1435, doi:10.1126/science.1110252.

Haywood, J. M., A. Jones, N. Bellouin, and D. Stephenson (2013), Asymmetric forcing from stratospheric aerosols impacts Sahelian rainfall, *Nat. Clim. Change*, *3*, 660–665, doi:10.1038/nclimate1857.

Held, I. M., and B. J. Soden (2006), Robust responses of the hydrological cycle to global warming, *J. Clim.*, *19*, 5686–5699.

Hu, Y., and Q. Fu (2007), Observed poleward expansion of the Hadley circulation since 1979, *Atmos. Chem. Phys.*, *7*, 5229–5236.

Jarvis, A. (2011), The magnitudes and timescales of global mean surface temperature feedbacks in climate models, *Earth Sys. Dyn.*, *2*, 213–221, doi:10.5194/esd-2-213-2011.

Johanson, C. M., and Q. Fu (2009), Hadley cell widening: Model simulations versus observations, *J. Clim.*, *22*, 2713–2725, doi:10.1175/2008JCLI2620.1.

Jones, A., et al. (2013), The "termination effect" in experiment G2 of the Geoengineering Model Intercomparison Project (GeoMIP), *J. Geophys. Res. Atmos.*, doi:10.1002/jgrd.50762.

Josey, S. A., E. C. Kent, D. Oakley, and P. K. Taylor (1996), A new global air-sea heat and momentum flux climatology, *Int. WOCE Newsletter*, *24*, 3–5.

Josey, S. A., E. C. Kent, and P. K. Taylor (1999), New insights into the ocean heat budget closure problem from analysis of the SOC air-sea flux climatology, *J. Clim.*, *12*, 2856–2880.

Joshi, M., and J. Gregory (2008), Dependence of the land-sea contrast in surface climate response on the nature of the forcing, *Geophys. Res. Lett.*, *35*, L24802, doi:10.1029/2008GL036234.

Joshi, M., J. M. Gregory, M. J. Webb, D. M. H. Sexton, and T. C. Johns (2008), Mechanisms for the land/sea warming contrast exhibited by simulations of climate change, *Clim. Dynam.*, *30*(5), 455–465, doi:10.1007/s00382-007-0306-1.

Kravitz, B., A. Robock, O. Boucher, H. Schmidt, K. E. Taylor, G. Stenchikov, and M. Schulz (2011), The Geoengineering Model Intercomparison Project (GeoMIP), *Atm. Sci. Lett.*, *12*, 162–167, doi:10.1002/asl.316.

Kravitz, B., et al. (2013), Climate model response from the Geoengineering Model Intercomparison Project (GeoMIP), *J. Geophys. Res. Atmos.*, *118*, 8320–8332, doi:10.1002/jgrd.50646.

Lambert, H., and M. J. Webb (2008), Dependency of global mean precipitation on surface temperature, *Geophys. Res. Lett.*, *35*, L16706, doi:10.1029/2008GL034838.

Liepert, B. G., and M. Previdi (2009), Do models and observations disagree on the rainfall response to global warming?, *J. Clim.*, *22*, 3156–3166, doi:10.1175/2008JCLI2472.1.

Lorenz, D. J., and E. T. DeWeaver (2007), The response of the extratropical hydrological cycle to global warming, *J. Clim.*, *20*, 3470–3484, doi:10.1175/JCLI4192.1.

Lu, J., G. A. Vecchi, and T. Reichler (2007), Expansion of the Hadley cell under global warming, *Geophys. Res. Lett.*, *34*, L06805, doi:10.1029/2006GL028443.

Matthews, H. D., and K. Caldeira (2007), Transient climate-carbon simulations of planetary geoengineering, *Proc. Natl. Acad. Sci. U.S.A.*, *104*(24), 9949–9954, doi:10.1073/pnas.0700419104.

Moreno-Cruz, J. B., K. L. Ricke, and D. W. Keith (2012), A simple model to account for regional inequalities in the effectiveness of solar radiation management, *Clim. Change*, *110*, 649–668, doi:10.1007/s10584-011-0103-z.

Muller, C. J., and P. A. O'Gorman (2011), An energetic perspective on the regional response of precipitation to climate change, *Nat. Clim. Change*, *1*, 266–271, doi:10.1038/nclimate1169.

Naik, V., D. J. Wuebbles, E. H. DeLucia, and J. A. Foley (2003), Influence of geoengineered climate on the terrestrial biosphere, *Environ. Management*, *32*(3), 373–381, doi:10.1007/s00267-003-2993-7.

O'Gorman, P. A., and T. Schneider (2008), The hydrological cycle over a wide range of climates simulated with an idealized GCM, *J. Clim.*, *21*, 3815–3832, doi:10.1175/2007JCLI2065.1.

O'Gorman, P. A., R. P. Allan, M. P. Byrne, and M. Previdi (2012), Energetic constraints on precipitation under climate change, *Surv. Geophys.*, *33*, 585–608, doi:10.1007/s10712-011-9159-6.

Ramanathan, V. (1981), The role of ocean–atmosphere interactions in the CO_2 climate problem, *J. Atmos. Sci.*, *38*, 918–930, doi:10.1175/1520-0469(1981)038<0918:TROOAI>2.0.CO;2.

Ricke, K. L., M. G. Morgan, and M. R. Allen (2010), Regional climate response to solar-radiation management, *Nat. Geosci.*, *3*, 537–541, doi:10.1038/ngeo915.

Rind, D., and W. B. Rossow (1984), The effects of physical processes on the Hadley circulation, *J. Atmos. Sci.*, *41*, 479–507, doi:10.1175/1520-0469(1974)041<0479;TEOPPO>2.0.CO;2.

Robock, A., L. Oman, and G. L. Stenchikov (2008), Regional climate responses to geoengineering with tropical and Arctic SO_2 injections, *J. Geophys. Res.*, *113*, D16101, doi:10.1029/2008JD010050.

Schmidt, H., et al. (2012), Solar irradiance reduction to counteract radiative forcing from a quadrupling of CO_2: Climate responses simulated by four Earth system models, *Earth Sys. Dyn.*, *3*, 63–78, doi:10.5194/esd-3-63-2012.

Schneider, T., P. A. O'Gorman, and X. J. Levine (2010), Water vapor and the dynamics of climate change, *Rev. Geophys.*, *48*, RG3001, doi:10.1029/2009RG000302.

Sellers, P. J., et al. (1996), Comparison of radiative and physiological effects of doubled atmospheric CO_2 on climate, *Science*, *271*, 1402–1406.

Shepherd, J., et al. (2009), Geoengineering the climate: Science, governance, and uncertainty, Royal Society Policy document 10/09, 82 pp.

Sutton, R. T., B. Dong, and J. M. Gregory (2007), Land/sea warming ratio in response to climate change: IPCC AR4 model results and comparison with observations, *Geophys. Res. Lett.*, *34*, L02701, doi:10.1029/2006GL028164.

Taylor, K. E., R. J. Stouffer, and G. A. Meehl (2012), An overview of CMIP5 and the experiment design, *Bull. Am. Meteorol. Soc.*, *93*, 485–498, doi:10.1175/BAMS-D-11-00094.1.

Tilmes, S., et al. (2013), The hydrological impact of geoengineering in the Geoengineering Model Intercomparison Project (GeoMIP), *J. Geophys. Res. Atmos.*, *118*, 11,036–11,058, doi:10.1002/jgrd.50868.

Trenberth, K. E., and A. Dai (2007), Effects of Mount Pinatubo volcanic eruption on the hydrological cycle as an analog of geoengineering, *Geophys. Res. Lett.*, *34*, L15702, doi:10.1029/GL2007GL030524.

Wang, K., and S. Liang (2009), Global atmospheric downward longwave radiation over land surface under all-sky conditions from 1973 to 2008, *J. Geophys. Res.*, *114*, D19101, doi:10.1029/2009JD011800.

Wild, M., and B. Liepert (2010), The Earth radiation balance as driver of the global hydrological cycle, *Environ. Res. Lett.*, *5*, 025003, doi:10.1008/1748-9326/5/2/025003.